OVERVIEW OF THE NSTX-U RECOVERY PROJECT PHYSICS AND ENGINEERING DESIGN

S. P. Gerhardt
Princeton Plasma Physics Laboratory
Princeton, USA
Email: sgerhard@pppl.gov

S.P. Gerhardt, J.E. Menard, C. Neumeyer, R. Feder, A. Adolfo, N. Atnafu, N. Allen, M. Awad, D. Battaglia, A. Basile, D. Bishop, W. Blanchard, A. Brooks, A. Brereton, M. Boyer, R. Burke, D. Cai, F. Cai, R. Camp, C. Ciummo, M. Cropper, M. D'Agostino, N. Dean, S. DePasquale, J. Dellas, D. Downing, L. Dudek, P. Dugan, R. Ellis, K. Erickson, J. Feng, N. Ferraro, C. Freeman, A. Gao, N. Greenough, J. Guttenfelder, F. Hoffmann, M. Jaworski, F. Jones, M. Kalish, A. Khodak, A. Jariwala, B. Jedic, J. Klabacha, I. Kunsch, M. Kumar, B. Linn, D. Loesser, F. Malinowski, J. Malo, M. Mardenfeld, J. Mitchell, C. Pagano, J.-K. Park, J. Petrella, W. Que, S. Raftopoulos, V. Riccardo, T. Ronge, M. Safabakhsh, H. Schneider, P. Sichta, M. Smith, B. Stratton, M. Sibilia, T. Stevenson, M. Styer, G. Swider, G. Tchilinguirian, P. Titus, M. Viola, W. Wang, T. Willard, I. Zatz, G. Zimmer, Y. Zhai, H. Zhang, X. Zhao
Princeton Plasma Physics Laboratory (PPPL)
Princeton, USA

M.L Reinke, T. Gray, D. Youchison
Oak Ridge National Laboratory
Oak Ridge, USA

Abstract

The NSTX-U Recovery Project is working to return NSTX-U to physics operations after a series of technical issues. New inner poloidal field coils are being fabricated, utilizing a design that lacks an intrinsic mandrel; this choice facilitates turn-to-turn testing. These coils are being supported by new "slings", which provide restraint against sideways and vertical loads, and also provide pre-load to the coils. Double O-ring seals are being implemented on large flanges between the CS and the outer vessel. New graphite plasma facing components are being implemented, to meet stringent heat flux and disruption requirements. Upgrades are being made to the bakeout system and the test cell neutron shielding. New mechanical instrumentation is being instituted for mechanical model validation and trending of machine performance. These activities are expected to enable the 2 MA, 1 T, 5 second flat-top operation with neutral beam heating up to 10 MW to support the full range of physics research envisioned for the upgraded NSTX facility.

1. INTRODUCTION

The National Spherical Torus Experiment (NSTX) [1] operated between 1999 and 2010, pursuing research across a broad range of physics and technology [2-4]. In 2010, the facility was shut down for a major upgrade, composed of two elements [5]: ii) a new central magnet assembly composed of a TF inner bundle, an OH solenoid, inner PF coils and associated components, and ii) the addition of a second neutral beam line. These facilitate the study of non-inductive current drive, the collisionality dependence of transport, fast-ion physics, and advanced divertor geometry [5]. NSTX-Upgrade (NSTX-U) operated for a 10-week period in 2016 [6,7]. However, the failure of an inner poloidal field (PF) coil necessitated the end of the run campaign.

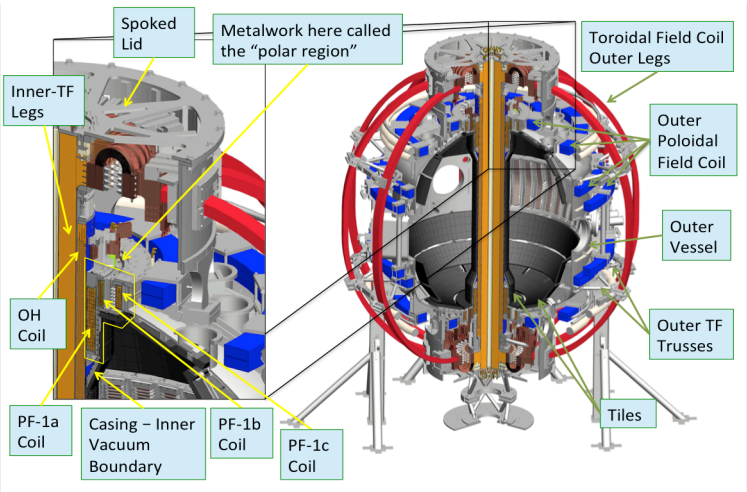

Fig 1: Overview of NSTX-U device

The PF coil failure, in addition to a number of other more modest technical issues, led the Department of Energy (DOE) to request Princeton Plasma Physics Laboratory (PPPL) complete an Extent of Condition (EoC) analysis and develop a Corrective Action Plan (CAP). The EoC process was composed of 12 Design Verification and Validation Reviews (DVVRs), each of which focused on a subset of the full technical scope of the experimental infrastructure (e.g. magnets, vessel and internal hardware, heating systems, etc.). These DVVRs identified repairs and enhancements required to restore high-reliability operations to NSTX-U over its full original proposed operating space (I_p=2 MA, B_T=1 T, Δt=5 s, P_{NBI}=10 MW). These issues, as well as the Project's proposed resolutions, were reviewed by an international panel of tokamak experts (the EoC committee) in two separate meetings.

The primary set of issues identified by the EoC process, and being addressed by the Recovery Project as the manifestation of the CAP, are as follows:

— Replace the inner-PF coils with new improved designs (Section 2)
— Update components of the "polar region", the vessel regions at the top and bottom, to accommodate new mandrel free inner-PF coils, to eliminate the lower ceramic insulator, and to accommodate double O-ring seals (Sect. 3)
— Update plasma facing components to handle full halo current and thermal loads (Sect. 4)
— Improvements to the passive plates (Sect. 5)
— Improvements to the bakeout system (Sect. 6)
— Improve machine instrumentation (Sect. 7)
— Upgrades to the test cell shielding (Sect. 8)

Note that the designs of these components are generally at the Preliminary Design Review (PDR) stage. Therefore, some design evolutions may occur before final fabrication and installation.

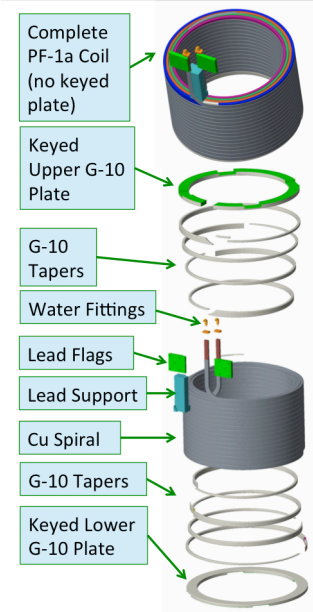

Fig. 2: Overview of inner-PF magnet construction.

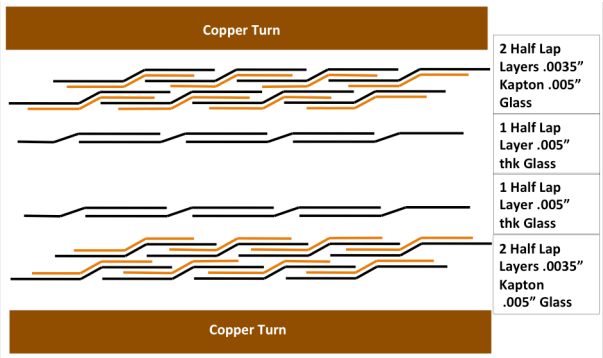

Fig. 3: Details of the inner-PF turn insulation.

2. NEW INNER-PF COILS

The upgraded centerstack for NSTX-U had three upper inner-PF coils, and three reflection-symmetric lower coils (See Fig. 1). The PF-1aU coil experienced a gradual layer-to-layer failure during the FY-16 run campaign. The final state of the failure involved a breach of the conductor wall. The coil was fabricated using a Cu conductor extruded with a cooling channel; a blockage of water flow from melted Cu was the first external sign of the fault. Subsequent forensic analysis found a region of "dry" insulation in the vicinity of the failure, where the vacuum pressure impregnation (VPI) apparently failed to draw in resin [8]. While this likely contributed to the failure, it was not possible to conclusively determine a single root cause. Given that all six inner-PF coils were purchased at the same time, and from the same manufacturer, it was deemed wise by the EoC Committee to replace all six inner-PF coils. Additionally, given that a layer-to-layer fault compromised the original NSTX-U PF-1aU coil, the committee recommended manufacturing the coils without permanent mandrels, so that precise inductance measurements and turn-to-turn insulation testing could be done.

TABLE 1. Turn-to-turn voltage and high-pot safety factors, based on 2 kV power supply terminal voltage

Coil	# of Layers	Layer-to-Layer Voltage [V]	Layer-to-Layer Safety Factor	High-Pot Voltage [V]	High-Pot Voltage Safety Factor
PF-1a	4	1012	72	5051	22
PF-1b	2	2025	36	9103	12
PF-1c	2	2025	32	9103	12

A model of the assembled PF-1a coil, and an exploded view of the coil, are shown in Fig. 2; the design features of the PF-1b and PF-1c are conceptually similar. The coil is a simple spiral,

unlike the previous coils that confined the row-transitions to a small toroidal angle. Custom machined G11 pieces are used at the top and bottom of the coil to provide a proper base or top to the spiral, to control the transition from layer to layer, and to fill all voids to avoid resin-rich regions.

The turn insulation scheme is shown in Fig. 3. Each conductor has two half-lapped layers of co-wound 0.0035" kapton with adhesive and 0.005" fiberglass, with an additional half-lapped layer of 0.005 fiberglass then applied to each conductor. The kapton is narrower than the fiberglass, which, along with the pattern indicated in Fig. 3, ensures that there is a complete wicking path through the insulation system for the CTD-425 hybrid insulation system. This insulation results in the turn-to-turn voltage safety factors noted in Table 1. The ground insulation is provided by seven half-lap layers of 0.012" thick glass, in addition to the turn insulation noted above. This provides the safety factors noted in Table 1 against the high-pot voltage, which is defined to be 2E+1 kV, where E is the maximum voltage to ground that the coil may experience during normal operations and fault scenarios.

The most challenging load case for the coils occur during cool-down; the coils are uniformly heated to their maximum temperature during the 5 second pulse (~60 C for the PF-1a, ~100 C for the PF-1b), then gradually cooled by 12 C water in the extruded cooling channel in the conductor [9]. This results in contraction of the cooled outer turns, with resulting stresses on both the copper and the insulation. While the conductor stress did not exceed the copper fatigue allowable, the insulation strains were judged unacceptably high. However, by applying a significant vertical pre-load (100 kips and 60 kips for the PF-1a and -1b coils), the projected insulation strains were reduced to acceptable levels. These insulation strain levels, which are limited to very small areas, were within the envelope of recent test data; samples of the OH coil insulation system, which is identical to that in the inner-PF coils, were subjected to 30k cycles at 0.6% strain and subsequently passed all electrical tests.

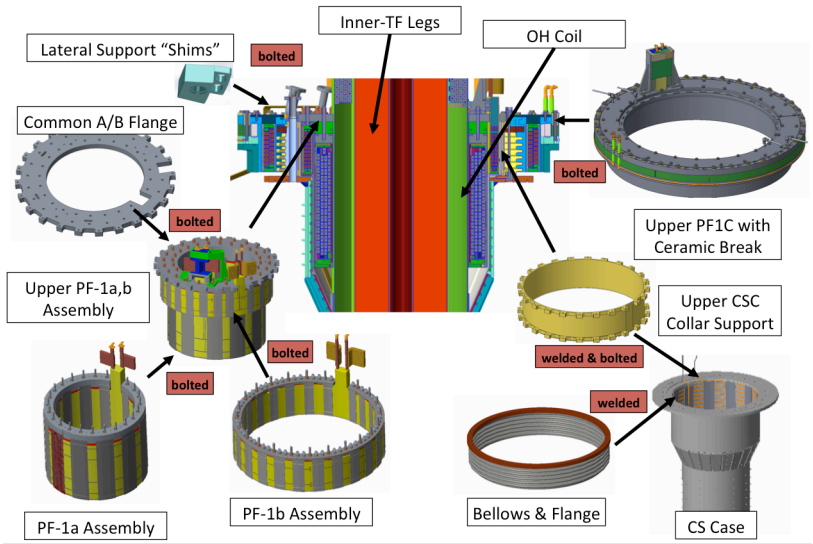

Fig. 4: Overview of the Polar Region Components

3. IMPROVED POLAR REGION COMPONENTS

As indicated in Figs. 1, 4, & 6, the "polar region" includes the highly complex components at the top and bottom of the machine that, among other goals, form the vacuum boundary and support the coils. The details of the polar region installation are provided in Fig. 4, where the installation at the bottom of the device largely mimics the installation at the top. Key elements include:

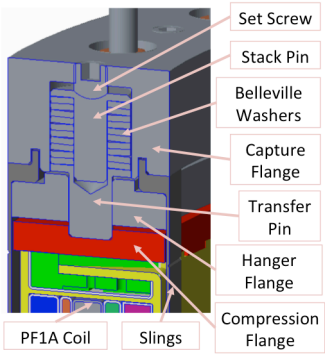

Fig. 5: Details of the inner-PF coils preload mechanism

- Each of the PF-1a and PF-1b coils is installed in a set of Inconel 718 "slings" which provide support for the coils. These assemblies are bolted to the Common A/B flange, which supports both coils.
- The PF-1c coils are embedded in a reentrant flange, with a cap to locate them within the flange. The flange has double O-ring seals on both its large and small major radius sides.
- The horizontal flange of the casing has attached to it both i) a bellows & flange, and ii) the Collar Support.
- The Collar Support provides a means of attaching the Common A/B flange to the CS casing.

Additional details of the sling design are shown in Fig. 5, where the PF-1a coil is used for the example. Radial keys are machined in the tops of the coil, which engage with keys in the compression flange. The Inconel 718 slings are trapped in grooves between the Hanger Flange and the Capture Flange. When the setscrew is turned, it

compresses the transfer pin via the stack pin, resulting in the coil being pressed into the slings. The Belleville washer stack is used to control the pre-load to the values required by the magnet design.

In the initial NSTX-U design, the PF-1b coil mandrel was directly connected to the CS casing. This results in i) larger thermal stresses at the interface between the coil mandrel and the casing, and ii) unacceptably high temperatures on the ground insulation of the coil during bakeout. In the new design, the -1b and -1a coils are supported by the Collar Support and a layer of microtherm insulation placed between the coils and casing, providing thermal isolation.

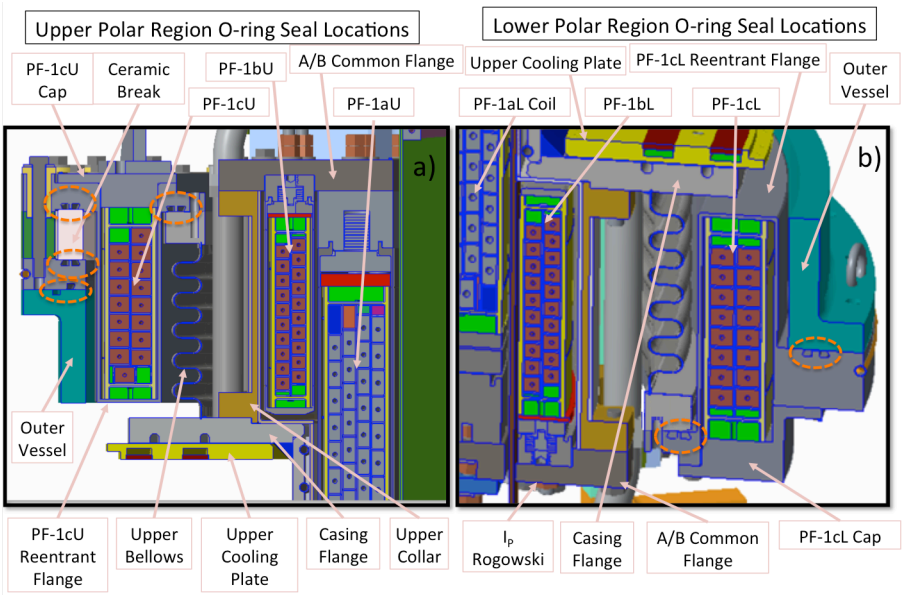

Fig. 6: Details of the polar region seals and assembly. See text for details

A key recommendation from the EoC committee was to eliminate the lower ceramic insulator, and to provide double O-rings for all the large vacuum seals. The motivation for removing the lower insulator were two-fold: 1) to eliminate potential leaks or failures associated with that insulator, and 2) to ensure that lithium associated with the research program does not come in contact with the alumina. The detailed manifestations of this recommendation are shown in Fig. 6. The top polar region has a single alumina insulator, with double O-rings on each face. This insulator is required to support the bakeout scheme, which runs 8 kA of DC current down the CS casing. G-7 insulators on the large radius side of the insulator ensure that the metal-to-ceramic contact cannot occur: the insulator "floats" on the O-rings. Note also that the insulator is installed between PF-1c reentrant housing and a separate flange, which bolt together as a sub-assembly (see Fig. 4 as well for an image of the complete sub-assembly). This design feature allows the insulator seals to be assembled and leak checked in a workshop away from the machine.

In addition to the double O-ring seals on the insulator, there are double-O ring seals where the bellows flanges mate to the PF-1c reentrant flanges. These O-ring grooves have a "dove-tail" configuration, to ensure that the O-rings do not fall out of their grooves during assembly. There are also double O-ring seals at the interface to the outer vacuum vessel. The outer vessel has an existing single O-ring groove at the upper interface, and therefore only a single additional groove is required on the ceramic insulator assembly flange. A dedicated pumping system is being designed to pump the interspaces of these double O-ring installations. Note that in addition to increasing the reliability of these seals while reducing the permeation rate, these double O-ring installations allow the seals to be leak checked before full machine pump-down.

A final key addition to the polar region is a dedicated cooling plate on the horizontal target, visible in Figs. 6 and 7. This plate is fabricated as two Inconel 625 components spanning just less than 180 degrees toroidal. The PFC mounting structures will be mounted to this plate (see next Section). Embedded cooling channels in the plate will use gaseous He cooling; water cooling is not allowed inside the NSTX-U vessel due to the potential for reaction with lithium in the event of a leak.

4. NEW PLASMA FACING COMPONENTS

The original graphite plasma facing components fielded for NSTX-Upgrade had a number of issues: their fastening scheme was in many cases not robust with regard to electromechanical loads due to halo currents, while leading edges and pre-loads resulting from the PFC attachment scheme severely limited the allowed heat fluxes. Therefore, the Recovery Project is implementing improvements to all PFC regions on the inner and outer divertors, both upper and lower, and center stack first wall.

The engineering scope of this work is broken into two general areas. The high heat flux (HHF) regions are the inboard divertor vertical (IBDV), inboard divertor horizontal (IBDH), and outboard divertor rows 1 & 2 (OBD12); see Fig. 7a) for labels on these regions. The low heat flux (LHF) tiles are located on the center stack angled (CSA) section, the center stack first wall (CSFW), and the outer rows of the outboard divertor (OBDR3,4,5). Note that there is a single row of low heat flux tiles at the interface between the IBDV and IBDH; the locations of divertor coils render it near-impossible to place either inner or outer strikepoints on this tile.

Isotropic graphite has been chosen for manufacture of all PFCs associated with Recovery; high-Z metal tiles are of interest for the long-term research program of the device, but were considered inappropriate for the initial research phase. Achievement of the lowest collisionality is critical to near-term NSTX-U research and this may not be achievable with excessive radiation from high-Z impurities reducing the net power or requiring operating at high separatrix density to mitigate erosion. Carbon-carbon composites were also considered, but not selected at this time due to cost and long material procurement times.

The tiles in the HHF region are subject to direct plasma heating from the inner or outer strikepoints, with time averaged perpendicular heat fluxes of order or exceeding ~10 MW/m^2 projected for some attached divertor scenarios even with large poloidal flux expansion or rapid strikepoint sweeping. It is not possible to design PFCs with isotropic graphite to meet a heat flux of this magnitude for pulse lengths of 5 seconds using isotropic graphite, assuming the 1600 C surface temperature limit adopted by the project. However, two strategies have been adopted in order to ensure reliable behavior of the tiles in the presence of the large heat fluxes:

— The tiles have a grid-like pattern machined on the top surface, such that the top of the tiles appear to be made of many smaller tiles; this process is known as castellation and is visible in the IBDV tiles in frames b) and c) of Fig. 7 or the IBDH tiles in frame d). The gaps between individual castellations on a given tile are 0.51 mm with a typical castellation area of ~2.5 cm x 2.5 cm (the exact dimension depend on the tile variant) and a typical castellation depth of ~2.5 cm. As indicated in Fig. 7d), the castellations have features at their base to eliminate what would otherwise be larger stress risers at the base of the slit. As illustrated in frame d) of Fig. 7, the use of castellations results in reduced surface compressive stress for a given surface temperature, or alternatively, allows the tiles to reach sublimation-driven surface temperature limits before any stress allowable (1/2 of ultimate) is reached. This has been demonstrated experimentally via e-beam testing on castellated graphite [10]. In particular, the end-of-pulse thermal stresses are shown, where the maximum magnitude surface compressive stress of 59 MPa should be compared to the ultimate strength of 130 MPa. Note that the larger castellations in the figure, which correspond in reality to a region of lower heat flux, show somewhat larger stresses in this model case with uniform heat flux across the tile.

— The tiles are “fishscaled”, so that heat coming in parallel to the field lines never strikes the vertical surfaces between castellations or between adjacent tiles. Parallel heat fluxes in excess of 300 MW/m^2 were estimated, and tile shaping prevents excessive temperature and stress on the leading edges. For maximum field line incident angles of 5 degrees and achievable manufacturing tolerances on the tiles and their backing structures, fish-scale angles of ~1 degree are used. This comparatively steep angle results in heat flux enhancement factors of ~2 for the low field line angle cases originally envisioned [5].

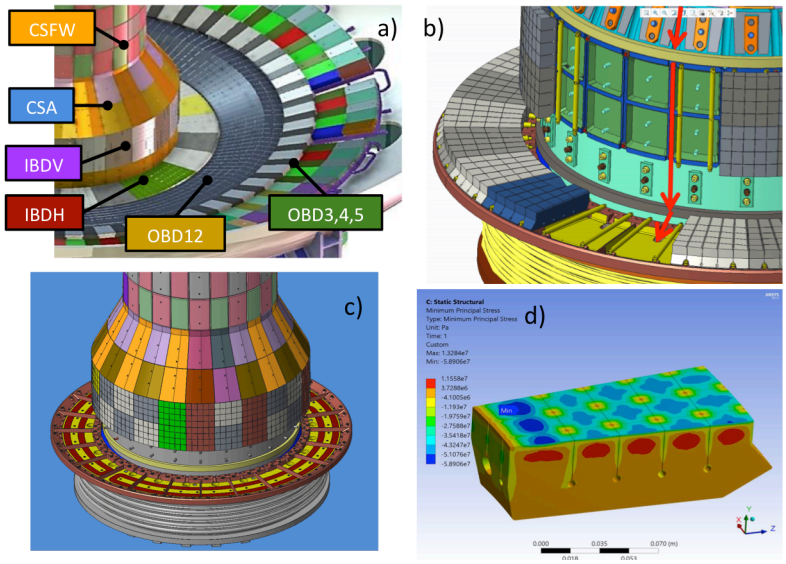

Fig. 7: Overview of the new PFC design. Frame a) labels the various tile regions, while frame b) and c) show the mounting structures for the IBDV and IBDH PFCs. Frame d) shows the end-of-pulse thermal stress state for a castellated tile.

These IBDV and IBDH high heat flux tiles are supported in tray structures, as illustrated in Fig 7 b) and c). The trays are mounted either to the top of the heat transfer plate, or to the vertical section of the casing. Rods with cams are used to secure the tiles, pulling them against grafoil sheets with pre-load controlled by Belleville washer stacks. The single row of low heat flux tiles at the interface between these regions allows the cam actuators for both tiles region to be hidden, such that there are no surface features associated with mounting hardware on the surface of the HHF tiles. Note that the OBDR12 tiles have a slightly different mounting system, while still eliminating all front-surface holes associated with mounting hardware.

The LHF tile regions are potentially subjected to large disruption loads, but reduced thermal demands. For these tiles, the previous T-bar or tray/pin schemes are retained, but with targeted modifications to improve performance. These include a larger-radius restraining pin to prevent the tiles from sliding along the T-bar, improved edge chamfers, and fabrication from a stronger graphite material than the original tiles.

The new high heat flux tiles are augmented with extensive diagnostics to support both operations and the physics program. These include thermocouples embedded within individual castellations which act as calorimeters. All divertors are instrumented, with additional toroidal locations instrument to provide redundancy and look for low-n toroidal variation caused my misalignment between the inner-PF coils and the PFCs. Optimization of the thermocouple geometry is ongoing: placing the thermocouple near the front surface of the castellation lead to the largest temperature rise for a given input energy, but can lead to unacceptable stress concentrations. Langmuir probes are installed in the gaps between individual castellations, with coverage at multiple toroidal angles in the divertor to provide redundancy while allowing the assessment of 3D effects. Magnetic diagnostics such as Mirnov sensors and Rogowski coils for halo current measurement on the center column are also being incorporated into the design.

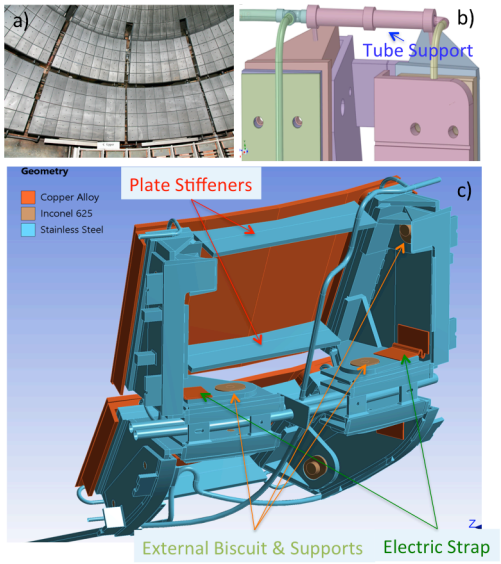

Fig. 8: Details of the passive plate improvements. See text for details.

5. IMPROVEMENTS TO THE PASSIVE PLATES

The passive plates, shown in Fig. 8a), are 0.5” thick Cu plates designed to provide passive stabilization to instabilities such as the n=0 vertical displacement event and the n=1 external kink. The plates are mounted to the vessel wall at each toroidal end of the plate, via a stainless steel bracket scheme that is designed to hold the plate while allowing for thermal growth of the plate during bakeout. The plate brackets are traced with stainless steel tubing, which facilitated bakeout of the passive plate graphite PFCs to 350 C. A number of issues were identified with the passive plates during and following the EoC process. Engineering remedies have been found for all of these issues. These issues include (see Fig. 8c):

— Excessive bending of the plates could occur during high current disruptions, challenging the strength of the Cu material. This is mitigated by the installation of stainless steel plate back stiffeners.
— Excessive stress could be applied to the welds on the brackets by the flexing of the plates during disruptions; the plate back stiffeners reduce that flexing and therefore reduce the stresses on the welds.
— Flex of the plates under disruption loads can result in excessive stresses on the passive plate graphite PFCs, which are mounted to the plates via T-bars. The plate back stiffeners mitigate this issue as well.
— The plates are mounted to their brackets via a mechanism that facilitates the thermal growth of the plates during bakeout. This involves a set of elliptical copper “biscuits” mounted in slides. When these were initially installed in the late 1990s, the holes in the biscuits were drilled overly large to accommodate the as-built field conditions of the vessel. The loose fit results in large plate motion in some cases, which can result in impact loads to components during disruption, as well as large loads on the He trace tubing. Rather than disassemble the full bracket assembly, which would require cutting and re-welding of all helium lines, a new “external” biscuit design has been created, which is installed in parallel with the existing bracketry.

This new design preserves the design intent of restraining motion from electromagnetic forces while accommodating thermal motion.

— Because each plate is mounted to the vacuum vessel via bracketry on each toroidal end of the plate, a net toroidal current can flow; this current facilitates vertical control of the plasma. However, part of this current path has been through the bolt & biscuit assembly, which is not designed to carry current. This presents a risk of arcing and potential make-break current paths. In order to mitigate the risk of arcing, dedicated "electric straps" are being installed at each interface between the plate and brackets, in parallel with the mechanical joint. These straps will have resistance sized to mitigate the potential for arcing at the biscuit while not being so low as to compromise the plasma startup.

— The large flux swing associated with disruption loads will also drive currents in the helium tubes. These currents have been computed, and it has been found that while tubes behind the plates are largely shielded, the tubes near the plate fronts can have substantial currents and therefore large electromagnetic loads. Therefore, the tubes need additional restraints at particular locations. An example of a restraint design is shown in Fig. 8b), where an electrically insulated clam-shell tube is attached to the helium tubes, then welded to the brackets via small support studs.

Overall, the improvements to the passive plate structures will mitigate all observed issues without mandating complete disassembly of the plate bracket and helium lines, with resulting cost and schedule savings.

6. IMPROVEMENTS TO THE BAKEOUT SYSTEM

The NSTX-U bakeout scheme is based on three systems: 1) distribution of up to 450 C helium through the backing structures of many PFCs, 2) passing up to 8 kA of current down the center column, providing Ohmic heating of the column, and 3) maintaining the vacuum vessel at 150 C via fluid passing through tubes on the vessel surface. Many features described in Sect. 3 will improve the bakeout performance of the device: the PF-1b coil is now thermally decoupled from the hot portions of the CS casing, and the heat transfer plate allows direct hot-He heating of the IBDH tiles.
Additional improvements being taken are as follows:

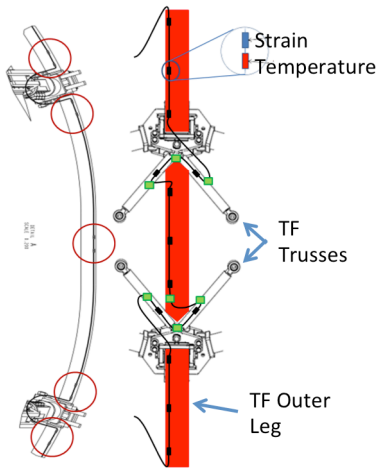

Fig. 9: Strain sensors on the outer-TF legs and outer-TF trusses.

— The insulation on hot-He pipes and manifolds is being repaired.

— The feedthroughs that pass hot-He through the vessel wall to the in-vessel tubing are not well designed to accommodate thermal stresses and are being evaluated. They may be qualified by empirical testing of the 304 SS under similar thermal and mechanical conditions, or new feedthroughs may be installed with improved design.

— Instrumentation and flow control values will be added to the ex-vessel hot-He distribution. This will allow the distribution of He to different points inside the vessel to be controlled, compensating for conductance variations that resulted in variations in the bakeout temperature.

— The ex-vessel fluid-based system was originally designed for a dielectric fluid with boiling temperature well above 150 C. However, the flammability of that fluid drove the design team to switch to water as the working fluid. When that switch was made, limited changes were made to the system to account for the lower boiling point of water. Recovery scope for this system involves installation of interlocks and redundant components to mitigate this so-called BLEVE (Boiling Liquid Expanding Vapor Explosion) risk.

7. IMPROVED MACHINE INSTRUMENTATION

The increase in performance to I_P=2 MA and B_T=1 T results in an approximate 4x increase in the various quasi-static and disruption loads applied to the device. While the device is designed to robustly withstand these increased loads, it is nevertheless prudent to apply instrumentation to various highly stressed components, in order to both validate models of the machine behavior underlying the design, and to trend behavior over time. In

general, the NSTX-U strain and displacement instrumentation is based on Fabry-Perot technologies for displacement measurements, and Fiber-Bragg technology for strain measurements; here the large channel count capability of the Fiber-Bragg technology is a large benefit. Note that the Fiber-Bragg measurements require temperature compensation, so a temperature sensor is often placed in near proximity to the strain sensor.

There are three general classes of measurements being made: i) the Preload Displacement Sensors, ii) the Global Torque Sensor via strain gauge arrays, and ii) the Outer PF Coil Displacement Sensors. The OH, PF-1a, and PF-1b coils utilize Belleville washer stacks to apply pre-load to the coils. A displacement sensor is used to monitor the preload on the OH coil. A sensor, not yet fully defined, will be used to measure the pre-load on the PF-1a and PF-1b coils. These sensors will monitor for a loss of preload due to creep or other factors, as well as confirm the bulk modulus and expansion coefficient of the coil packs.

A second class of measurements are related to the global torque balance of the machine. There is significant torque on the TF coils, due to their current crossing the poloidal field. Many structures are designed to transfer this torque to the vessel. As shown in Fig. 9, sensors will be placed along the regions of the TF outer legs with the highest strain. Furthermore, stain sensors will be placed on the trusses that support the TF; these outer leg and truss measurements can be made with a single string of sensors for each TF coil. This will allow an assessment of the accuracy of the model for the outer leg, while trending the outer leg behavior over time and allowing the truss uniformity to be assessed and optimized. Finally, a rosette of strain measurements will be placed on the inner-TF bundle itself to validate models of the torsional stiffness of the bundle, while trending the twist on the bundle as a function of time and load.

Finally, the outer-PF coils are supported from the vessel, on supports with slides that allow the thermal expansion of the vessel during bakeout, or thermal expansion of the coil during operations. These slides will be instrumented with displacement sensors to ensure that they are operating properly.

8. UPGRADES TO TEST CELL SHIELDING

The test cell within which NSTX-U resides was initially designed as a “hot cell” for tritium handling purposes, as well as a facility for a neutral beam testing. As such it had numerous doors and penetrations in the test cell walls, which allow 2.45 MeV neutrons from D-D reactions to escape to occupied areas of the building, or to the PPPL site boundary. Measurements during the 2016 run, and via a D-T generator after the run, have permitted a determination of the penetrations and doors that contribute the most to the dose outside the test cell.

Designs for improving the shielding at these locations have been made using the MCNP code. These involve construction of a concrete labyrinth in front of one of the problematic doors, and closing a legacy concrete door that had previously been abandoned in place to shield the other problematic door. The test cell windows, which had previously been simply covered by steel plates, will be filled with either concrete or polyethylene beads.

REFERENCES

[1] ONO, M., et al, Exploration of spherical torus physics in the NSTX device, Nuclear Fusion **40** (2000) 557

[2] GATES, D.A., et al., Overview of results from the National Spherical Torus Experiment (NSTX), Nuclear Fusion **49** (2009) 104016

[3] RAMAN, R., et al., Overview of physic results from NSTX, Nuclear Fusion **51** (2011) 094011

[4] SABBAGH, S.A., et al, Overview of physics results from the conclusive operation of the National Spherical Torus Experiment, Nuclear Fusion **53** (2013) 104007

[5] Menard Nuclear Fusion Paper on Upgrade

[6] BATTAGLIA, D., et al, Scenario Development During Commissioning Operations on the National Spherical Torus Experiment Upgrade, Nuclear Fusion **58** (2018) 046010

[7] MENARD, J., et al, Overview of first operational and physics results from NSTX-Upgrade, Nuclear Fusion **57** (2017) 102006

[8] PETRELLA, J., et al., Forensic Analysis of Faulted NSTX-U Inner Poloidal Field Coil, IEEE Transactions on Plasma Science **46** (2018) 2653.

[9] ZHAI, Y. et al., Inner PF Coil Thermal Analysis, NSTXU-CALC-133-27, PPPL, Princeton, USA, 2018.

[10] GRAY, T. et al, Integrated plasma facing component calorimetry for measurement of shot integrated deposited energy in the NSTX-U Spherical Torus, Rev. Sci. Instrum, Accepted (2018)